ADVANCED MATERIALS
www.advmat.de

Voltage-Controlled Nonvolatile Molecular Memory of an Azobenzene Monolayer through Solution-Processed Reduced Graphene Oxide Contacts

Misook Min, Sohyeon Seo, Sae Mi Lee, and Hyoyoung Lee**

Solution-processed fabrication of molecular devices without the use of lithographic techniques is currently a major goal in plastics-based molecular electronics. Reduced graphene oxide (rGO),[1–3] a single-layer sp^2-carbon atomic sheet that is electronically compatible with graphene, has attracted attention because of its excellent solution dispersion and its semimetallic property of high conductivity, which allows good electronic contacts with organic molecules.[4,5] Like noble metals, graphene can act as a building block for molecular assembly using bottom-up fabrication and can provide chemically compatible contacts via the formation of carbon–carbon bonds[6] and stable contacts that avoid contact fluctuations at the interface with organic molecules.[3] The abundant supply of electrons on graphene can react with electrophilic groups (e.g., via a dediazoniation process with diazonium molecules) to assemble a monolayer (i.e., self-assembled monolayers, SAMs), which are highly ordered arrays of molecules on a two-dimensional (2D) graphene surface with a chemisorbed bottom contact.[7] The application of a second contact on top of the molecular SAM can form 2D monolayer molecular junctions across the molecules on the graphene bottom contact, which is the typical structure of crossbar-type molecular devices consisting of molecular SAMs sandwiched between two electrodes.[8–10] Such molecular devices can exhibit technological advantages and manifest various operating mechanisms regarding molecular functions. For the realization of molecular devices, new, simple, and suitable operating mechanisms are of interest. In particular, the molecules used for many molecular-electronics studies have been molecular switches that can be simply operated with light or an applied electric field.[3,11,12] For example, azobenzene (AB) has been the most frequently utilized candidate that displays two conformational isomers for molecular switches.[13–16] The operation of an AB molecular switch in monolayer molecular junctions requires conducting contacts with sufficient flexibility to adopt to the height change of an AB SAM due to the *trans–cis* isomerization of the N=N double bond.

Herein, an rGO solution process for the fabrication of a flexible molecular monolayer electronic device is designed that allows the generation of a physical soft top contact to AB molecules covalently attached to an rGO bottom contact (**Figure 1**a). A graphene oxide (GO) film spin-coated onto a substrate was chemically reduced by hydrazine vapor to rGO, which results in a nucleophilic surface with a π electronic sp^2-hybrid carbon framework that can provide electrons to the electrophilic AB diazonium molecules. A second rGO contact was formed on top of the AB SAM by spray-coating with rGO solution. The length of the molecular junctions in the monolayer could be changed through the isomerization of AB (Figure 1b). The schematics in Figure 1b show the concept of voltage-induced *trans–cis* isomerization of AB molecules. Our hypothesis is that a specific bias voltage applied between two electrodes in a molecular junction can allow electron transmission between an electrode and AB molecules.[14] Changing *trans* isomers into *cis* isomers shortens the molecular junctions and causes the molecular conductance through the junctions to increase. In applications of prototype molecular monolayer switch devices with this type of simple operating mechanism, electrical switching due to differences in the molecular conductance of AB SAMs should be stable and rapid.

To reduce the steric hindrance due to the isomerization of adjacent AB molecules and increase the packing density of the AB SAM on the rGO bottom electrode, a long alkyl spacer was introduced between the AB moiety and the benzenediazonium moiety (i.e., (*E*)-4-(10-(4-((4-(trifluoromethyl)phenyl)diazenyl)phenoxy)decyloxy)benzenediazonium tetrafluoroborate, $ABC10N_2{+}BF_4^-$). We show reversible voltage-controlled isomerizations of ABC10 in a monolayer resulting in a reversible change of the surface friction and reversible conductance switching, with a change in the junction distance in rGO/ABC10 SAM/rGO devices that leads to a rewritable nonvolatile memory effect. The reliability of the molecular monolayer junctions between two rGO electrodes in a crossbar device is elucidated by molecular-length-dependent tunneling transport behavior across molecules.[17] In contrast to photoinduced *trans–cis* isomerization of AB molecules in monolayers or in solution, which takes from a few to several tens of minutes,[13,16] electric field[15] (or electron)[14]-induced isomerization occurs in a few seconds. The rapid current response to the voltage-controlled *trans–cis* isomerization of the rGO/ABC10 SAM/rGO devices showed stable nonvolatile memory performance, which

M. Min, Dr. S. Seo, S. M. Lee, Prof. H. Lee
Department of Chemistry
Sungkyunkwan University
300 Cheoncheon-dong,
Jangan-gu, Suwon, Gyeonggi-do, Republic of Korea
E-mail: sshyeon@skku.edu; hyoyoung@skku.edu
Prof. H. Lee
Department of Energy Science
Sungkyunkwan University
300 Cheoncheon-dong, Jangan-gu,
Suwon, Gyeonggi-do, Republic of Korea

DOI: 10.1002/adma.201303335

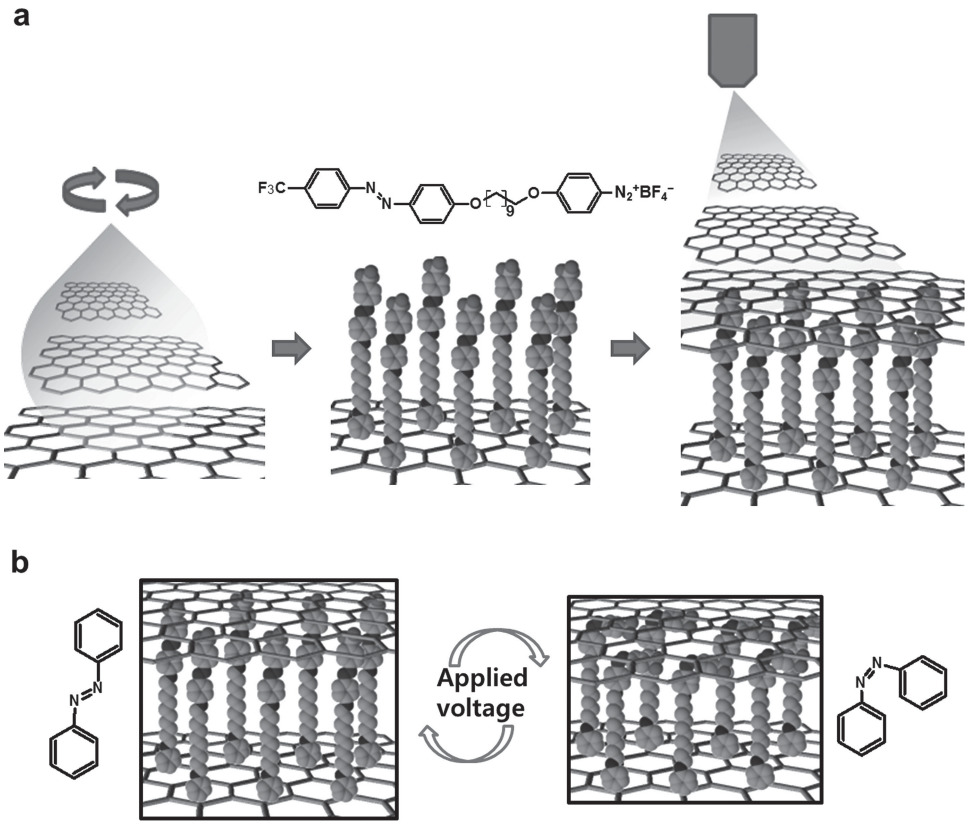

Figure 1. Illustration of a) solution-processed molecular-device fabrication and b) voltage-induced conductance switching between the two conductance states of the conformational isomers of the azobenzene (ABC10) molecules in a monolayer.

indicates that the rGO top contact has sufficient flexibility to respond to the height change of the ABC10 SAM.

Under an applied voltage, the *trans–cis* isomerization of AB molecules in ABC10 SAMs was detected by using a friction atomic force microscope (AFM), due to a change of the surface hydrophobicity in response to the difference between the hydrophobic surface with terminal CF_3 groups in the *trans* conformation and the hydrophilic surface with exposed N=N moieties in the *cis* conformation (**Figure 2**).[16] An ABC10 SAM was prepared on a highly doped p++ Si substrate as described in a previous report.[16] By using conducting-AFM (C-AFM), a selected area was scanned by the application of a bias voltage

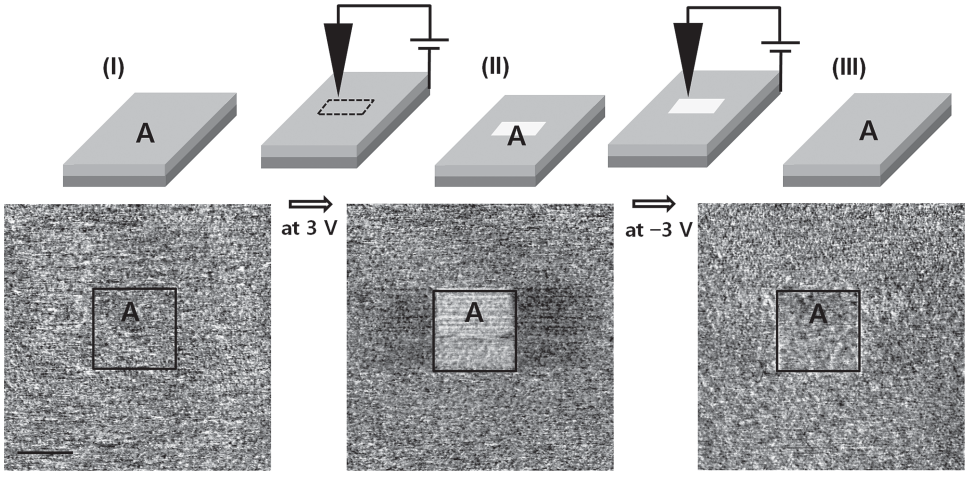

Figure 2. Schematic of the C-AFM measurement process and corresponding friction images of voltage-dependent conformational changes in an ABC10 SAM on Si. I) A friction image (scale bar, 1.1 μm) of the native ABC10 SAM, obtained at 0 V. II,III) Friction images, obtained at 0 V, over a larger area after scanning the area A at 3 and –3 V.

to the tip that can lead to the crossing over of the potential barrier between *trans* and *cis* states and trigger *trans–cis* isomerization at above-threshold biases.[14]

At 0 V, the native ABC10 SAM did not exhibit noticeable changes in the friction image (I), which indicates that the surface is entirely homogeneous for one isomer conformation (e.g., *trans* isomers). To induce a conformational change from *trans* to *cis* isomers, the tip was used to scan an area (e.g., $1.5 \times 1.5\ \mu m^2$) with an applied voltage of 3 V, which is in the scope of the required photon energy for photoisomerization (e.g., 2.8 – 3.9 eV).[14,18–20] After this, in an imaging scan over a larger area (e.g., $5.6 \times 5.6\ \mu m^2$) at 0 V, the friction over the previously scanned area was remarkably increased; this shows as a bright area in the friction image (II). In the *cis* transformation, the N=N moieties of ABC10, which are relatively hydrophilic compared to the terminal CF_3 groups, are exposed to the scanning tip and thus the surface friction between the tip and the N=N moieties increases.[21] The reverse conversion was induced by applying –3 V. The area scanned at –3 V, which was previously bright, showed the same friction as the surroundings in a friction image (III). Therefore, the *trans–cis* isomerization of ABC10 SAM can be achieved by the application of voltage (e.g., 3 V for *trans*-to-*cis* isomers and –3 V for *cis*-to-*trans* isomers). Consequently, the voltage-induced conformational isomerization between *trans* and *cis* states indicates that ABC10 molecules can act as a molecular switch triggered by transmitting electrons at above threshold biases. On the other hand, no noticeable changes in a surface height were observed in topographic images (Figure S1, Supporting Information) at each corresponding condition although the physical height of AB molecules should be changed by the isomerization, which is probably due to surface disturbance by the tip contacting the surface.

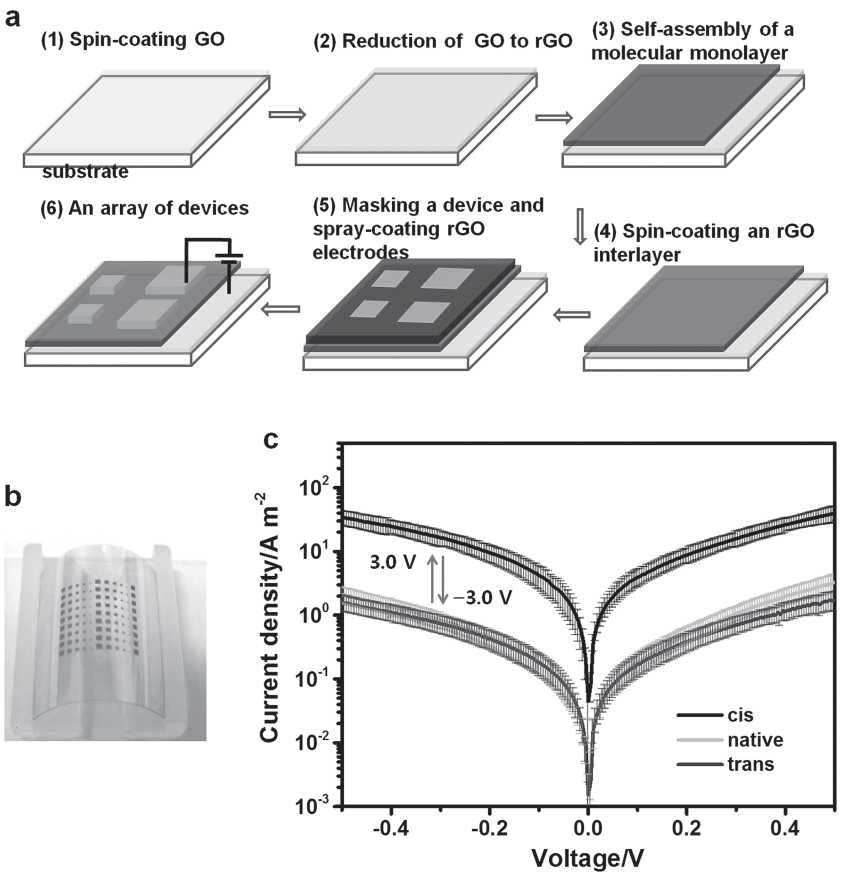

Figure 3. a) Schematic of solution-processed fabrication of rGO/molecular SAM/rGO devices. b) An optical image of an array of devices on a flexible plastic substrate. c) Current–voltage characteristics for voltage-driven reversible conductance switching of rGO/ABC10 SAM/rGO devices corresponding to two conformational states in a flat condition with flexible substrates. The voltages were swept from –0.5 to 0.5 V after applying voltages of 3 and –3 V to induce conformational changes from *trans–cis* isomers and *cis–trans* isomers, respectively. Current density plots were generated from average values obtained from over 50 devices (error bars denote standard deviations).

Voltage-controlled memory devices based on a molecular SAM on an rGO electrode were fabricated in an all-solution process (**Figure 3**a). An rGO bottom electrode was made by chemical reduction of a GO film on a plastic substrate (e.g., polyethylene terephthalate, PET) deposited with indium tin oxide (ITO) to conduct current to an electrical circuit for characteristic measurements (steps 1 and 2). To reduce the surface roughness, the surface condition of the rGO bottom electrode was controlled by the concentration of GO, the spin speed, and the number of the spin-coating times. As a result, the AFM image of the rGO bottom electrode chemically reduced from the spin-coated GO layer showed relatively lower surface roughness than the bare ITO/PET substrate (Figure S2), which indicates that the rGO bottom layer leveled off the ITO/PET surface. The root-mean-square (rms) surface roughness value was measured as approximately 1.6 nm for the rGO bottom electrode, which is similar to the value of 1.4 nm of an Au film normally used for molecular-electronic devices.[22] The thickness of the ABC10 SAM was measured at approximately 3 nm,[16] and the rGO bottom surface turned out to be enough to overcome an electrical breakdown (Figure S3a). In step 3, aryl diazonium salts were chemically attached to the rGO film using a self-assembling technique via C–C bonding with sp^2 carbon atoms in the rGO framework, which resulted in the formation of a monolayer. In step 4, an rGO interlayer was introduced to protect the molecular monolayer from the deposition of the top electrode with a relative abundance of rGO. Finally, the monolayer molecular junctions were completed by the formation of rGO top electrodes in step 5, which were patterned by spray-coating of rGO solution (Figure 3b). In molecular-electronic devices, the stability of molecular junctions definitely influences the device yield. A very thin rGO interlayer (approximately 1–2 layers) protected the molecular SAM well and assisted the thick rGO top electrode in stably contacting the molecular SAM. The device yield for ABC10 SAMs on rGO/ITO/PET was obtained

as approximately 60%, which can be an acceptable yield for molecular-electronic devices. Furthermore, cross-sectional scanning electron microscopy (SEM) images of rGO/ABC10 SAM/rGO/SiO_2 as a model device for rGO/ABC10 SAM/rGO showed welded (good; Figure S3a) or apart (bad; Figure S3b) molecular junctions of the ABC10 SAM between two rGO electrodes, which indicates that the reliability of the molecular junctions can be predominated by the physical contact of the top electrode including the thin rGO interlayer that should influence the stability of the electrical contact in the molecular devices.

To probe the monolayer molecular devices fabricated using the new process, three alkyl benzenediazonium salts with different alkyl backbones (4-octyl, 4-decyl, and 4-dodecyl benzenediazonium tetrafluoroborate) were used to fabricate rGO/alkyl benzene SAM/rGO devices as controls for the dependence of tunneling currents on the molecular junction distance, as is expected in rGO/ABC10 SAM/rGO devices. The alkyl benzene SAMs on the rGO electrodes demonstrated a new absorption peak at around 2910 cm^{-1} (sp^3 C–H stretch) in the Fourier-transform infrared (FT-IR) spectra (Figure S4a), which clearly indicated the presence of alkyl benzene molecules chemically bound to rGO. In addition, in the Raman spectra (Figure S4b), the intensity ratio of the D band (at around 1350 cm^{-1}) to the G band (at around 1590 cm^{-1}) increased from 1.15–1.17 to 1.19–1.22 after grafting alkyl benzene molecules onto rGOs, which indicates that structural defects in the C=C sp^2 graphene plane are generated due to C–C sp^3 bond formation.[7] Fabricated rGO/alkyl benzene SAM/rGO devices exhibited an exponential decrease in current density as molecular length increased (Figure S5); this reveals that electron transport via the molecular junctions between the two rGO electrodes followed a tunneling mechanism.[23,24] Current density (J) plots are described by $J \propto \exp(-\beta d)$, where β is the tunneling decay coefficient and d is the molecular length; the average β was 0.54 ± 0.02 $Å^{-1}$, which is much lower than that of alkanethiols (via a single Au–S contact) and slightly lower than those of oligophenylene thiols (via a single Au–S contact) and alkanedithiols (via double Au–S contacts).[8,23,25] Consequently, the new rGO/molecular SAM/rGO junction system can reliably perform molecular-tunneling transport through molecular monolayers.

With the identification of the formation of new C–C sp^3 bonds between ABC10 and rGO, the formation of an ABC10 SAM on rGO was characterized by X-ray photoelectron spectroscopy (XPS; Figure S6a) and transmission electron microscopy (TEM; Figure S6b). In the XPS spectra peaks corresponding to N=N (at about 400.0 eV, N 1s), C–F (at about 688.3 eV, F 1s), and C–N (at about 287.5 eV, C 1s) were identified,[16,26] revealing that ABC10 is chemically bound to rGO. In high-resolution TEM images, the lattice constant of rGO increased slightly after ABC10 modification (a = 2.80 ± 0.04 Å) when compared to that of pristine rGO (a = 2.44 ± 0.01 Å), which indicates that the expansion effect arose as C=C sp^2 bonds were rearranged to form covalent C–C sp^3 bonds.[27]

In the same manner to C-AFM measurements, voltage-induced ABC10 isomerization in rGO/ABC10 SAM/rGO devices was investigated by using voltage–current characteristic measurements. Figure 3c shows plots of current density against voltage for rGO/ABC10 SAM/rGO devices in different conformations after application of relevant voltages. As demonstrated in the rGO/alkyl benzene SAMs/rGO devices (Figure S5), tunneling currents across the molecular junctions in rGO/molecular SAM/rGO devices depend on the junction distance. As shown in Figure S5 for 4-alkyl benzene SAM devices, the length difference in an alkyl spacer of the molecules can dramatically affect a change in a junction resistance. The current densities of the 4-alkyl benzene SAM devices sharply decreased by over ten times with the addition of two methylene units, exhibiting a high sensitivity to alkyl-chain lengths. For the ABC10 SAM, the height difference between ABC10 isomers in their SAMs was estimated to be approximately 6.45 Å (obtained with the optimized 3D structures of *trans–cis* isomers by geometric modeling in ACD/Labs ACD/ChemSketch), which should cause a significant change in the resistance value between two isomer junctions, showing a large difference of over 15 times in the current-density plots (Figure 3c). Molecular tunneling junctions in the rGO/*trans*-ABC10 SAM/rGO devices exhibit a relatively low conducting state due to a longer junction distance than in the rGO/*cis*-ABC10 SAM/rGO devices. The transformation of these two molecular-conducting states is reversible, while devices with alkyl benzene molecules do not show voltage-induced molecular-conductance switching. In particular, rGO contacts allow reversible switching between *trans* and *cis* conformations, while very little conductance switching took place (even irreversibly) via the metal contact (e.g., gold top electrode/rGO interlayer/ABC10 SAM/Si bottom electrode; Figure S7). In molecular-electronic devices, the molecular interactions with the electrode (or contact) play a crucial role in electron transport across SAM junctions, as well as the contact geometry and the packing density of the monolayer.[28] Based on our results, adoption of the *cis* configuration in a densely packed monolayer with a gold top contact can cause a distortion of the monolayer structure to decrease in its reverse conversion, even though the top electrode is physically deposited on top of the rGO interlayer/ABC10 SAM. On the other hand, the conformational-change-dependent conductance switching of an ABC10 SAM was effectively performed with rGO soft contacts, providing clear evidence for the stability of rGO/ABC10 SAM/rGO devices.

Finally, the reversible *trans–cis* isomerization, which is controlled by a voltage pulse through the rGO/ABC10 SAM/rGO junction, was exploited for application in a nonvolatile memory device (**Figure 4**). The performances of the rGO/ABC10 SAM/rGO memory devices were tested at a voltage range between –4.0 and +4.0 V (Figure 4a). The voltage biased to the top electrode was swept from 0 to +4.0 and –4.0 V in a cycle. In contrast with the rGO/rGO device, which did not exhibit a current hysteresis loop, the rGO/ABC10 SAM/rGO devices showed significant current hysteresis loops due to resistive switching between the two states, which is consistent with the *trans*- (high resistivity) and *cis*- (low resistivity) states in Figure 3c. Furthermore, in a control device with azobenzene-free SAMs (e.g., a 4-dodecyl benzene SAM), no current hysteresis was observed in any 4-alkyl benzene SAM devices (Figure S8). Thus, in current–voltage plots, conductance switching from low (OFF state) to high (ON state) conducting states corresponds to switching between *trans* and *cis* conformations, respectively. At –1.0 V, the current value of the ON state was approximately 20 times larger than that of the OFF state, and this ratio was maintained

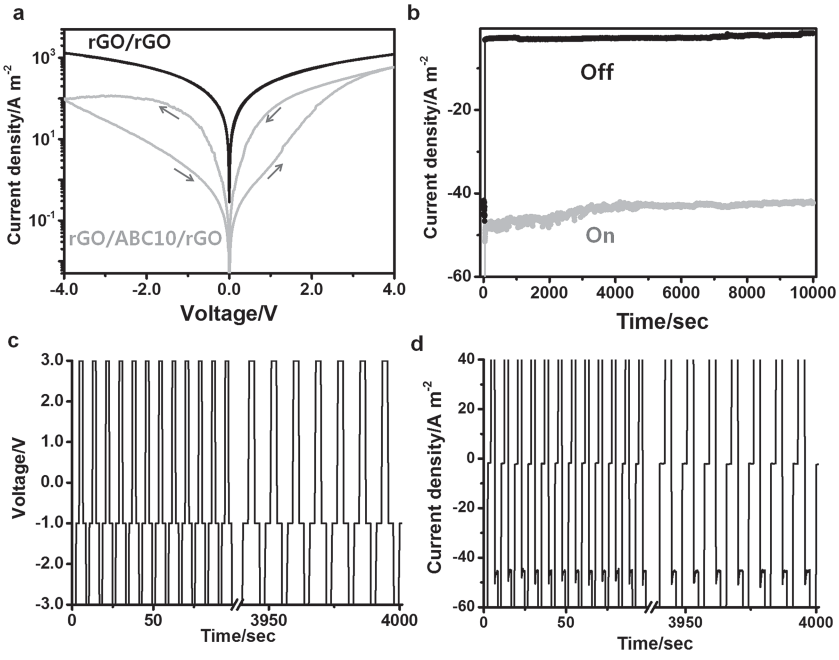

Figure 4. a) Current–voltage characteristics of the rGO/rGO device and the rGO/ABC10 SAM/rGO device; the voltage was swept from 0 to 4 V and to –4 V in a cycle. b) Memory-retention performances of the ON state and the OFF state at –1 V after applying voltages of 3 and –3 V, respectively. c) WRER performances at 3 , –1, –3, and –1 V (with 2 s of pulse width time) and d) their corresponding current responses.

for a retention time of >10000 s (Figure 4b). The nonvolatile memory performances of write–read–erase–read (WRER) were tested (Figures 4c and d). The voltages for writing, reading, and erasing were 3.0, –1.0, and –3.0 V, respectively (Figure 4c), and the memory operation was stable for over 400 cycles of WRER (Figure 4d). The WRER operation was preserved after six months of storage. Therefore, as shown in Figure 4, the devices demonstrated crucial characteristics for use as nonvolatile memory, showing stable retention and endurance of ON/OFF states; the rGO/ABC10 SAM/rGO memory devices showed clear ON/OFF states and nondestructive states over more than 20000 readouts for 10000 s (see continuous WRER performances in Figure S9). Furthermore, such flexible rGO/ABC10 SAM/rGO devices also showed good memory characteristics with applied bending stress (Figure S10).

In conclusion, the solution-processed fabrication of a molecular monolayer-based nonvolatile memory flexible device on a plastic substrate was successfully accomplished. We found that an rGO soft-contact top electrode can play an important role in the conformational-change-dependent conductance-switching process of an ABC10 SAM. Voltage-controlled *trans–cis* isomerizations of ABC10 molecules in a SAM were applied to an rGO/ABC10 SAM/rGO device, which showed stable nonvolatile memory operations.

Experimental Section

Materials and Characterization: GO was chemically synthesized from graphite and used to synthesize rGO as detailed in a previous study.[4] Aryl diazonium salts were also synthesized according to previously reported methods.[3] GO and rGO were characterized by AFM (Agilent 5100 AFM/SPM system), TEM (JEOL JEM-2100F), FTIR (Bruker IFS-66/S), Raman spectroscopy (514 nm, Reinshaw, RM1000-In Via), and UV-Vis spectroscopy (Shimadzu UV-3600 UV-Vis-NIR).[29–31]

Conducting-AFM Measurements: C-AFM was performed under ambient conditions (at a relative humidity of 25 ± 0.5% and room temperature). Pt-coated AFM tips were used.

Fabrication of rGO/Molecular SAM/rGO Devices: A GO film (spin-coated 3–4 times with a solution of 3.0 mg mL^{-1} GO in deionized water at 6000 rpm) was fully deposited on indium tin oxide (ITO)-coated PET substrates (60 Ω $sq.^{-1}$, Aldrich) after treatment of O_2 plasma of 100 W (5 $min)^{-1}$, and then reduced by hydrazine vapor to produce a ca. 6-nm rGO bottom electrode. The surface roughness of rGO-coated ITO/PET substrates was dramatically reduced (Figure S2). After grafting aryl diazonium salts on the rGO/ITO/PET substrate, an array of ca. 200-nm rGO top electrodes (ca. 200 × 200 μm^2 – 600 × 600 μm^2) was fabricated by spraying an rGO solution after spin-coating an rGO interlayer (approximately 1–2 layers with <0.5 mg mL^{-1} rGO in *N*,*N*-dimethylformamide at 4000 rpm) to protect the grafted molecular monolayers.

Fabrication of Au/Molecular SAM/Si Devices: ABC10 SAM-modified Si(111) surfaces were prepared according to literature procedures.[16] An array of 60-nm gold top electrodes (ca. 200 × 200 μm^2 – 600 × 600 μm^2) was fabricated by e-beam evaporation (at 0.1 Å s^{-1}) after spin-coating the rGO interlayer to protect the grafted molecular monolayers as described above.

Device Characterization: Electrical characteristics of the devices were measured with a Keithley 4200-SCS semiconductor characterization system under ambient conditions.

Supporting Information

Supporting Information is available from the Wiley Online Library or from the author.

Acknowledgements

This work was supported by the National Research Foundation of Korea (NRF) grant funded by the Korea government (MSIP; Grant No. 2006–0050684).

Received: July 19, 2013
Revised: August 14, 2013
Published online: October 17, 2013

[1] Y. Zhu, S. Murali, W. Cai, X. Li, J. W. Suk, J. R. Potts, R. S. Ruoff, *Adv. Mater.* **2010**, *22*, 3906.
[2] G. Eda, C. Mattevi, H. Yamaguchi, H. Kim, M. Chhowalla, *J. Phys. Chem. C* **2009**, *113*, 15768.
[3] J. He, B. Chen, A. K. Flatt, J. J. Stephenson, C. D. Doyle, J. M. Tour, *Nat. Mater.* **2006**, *5*, 63.
[4] S. Seo, M. Min, J. Lee, T. Lee, S. Y. Choi, H. Lee, *Angew. Chem. Int. Ed.* **2012**, *51*, 108.

[5] J. Liu, Z. Yin, X. Cao, F. Zhao, L. Wang, W. Huang, H. Zhang, *Adv. Mater.* **2013**, *25*, 233.
[6] M. Z. Hossain, M. A. Walsh, M. C. Hersam, *J. Am. Chem. Soc.* **2010**, *132*, 15399.
[7] H. Zhang, E. Bekyarova, J. W. Huang, Z. Zhao, W. Bao, F. Wang, R. C. Haddon, C. N. Lau, *Nano Lett.* **2011**, *11*, 4047.
[8] H. B. Akkerman, P. W. M. Blom, D. M. de Leeuw, B. de Boer, *Nature* **2006**, *441*, 69.
[9] S. Park, G. Wang, B. Cho, Y. Kim, S. Song, Y. Ji, M. H. Yoon, T. Lee, *Nat. Nanotechnol.* **2012**, *7*, 438.
[10] G. Wang, Y. Kim, M. Choe, T. W. Kim, T. Lee, *Adv. Mater.* **2011**, *23*, 755.
[11] A. J. Kronemeijer, H. B. Akkerman, T. Kudernac, B. J. Van Wees, B. L. Feringa, P. W. M. Blom, B. De Boer, *Adv. Mater.* **2008**, *20*, 1467.
[12] K. Seo, A. V. Konchenko, J. Lee, G. S. Bang, H. Lee, *J. Mater. Chem.* **2009**, *19*, 7617.
[13] V. Ferri, M. Elbing, G. Pace, M. D. Dickey, M. Zharnikov, P. Samor, M. Mayor, M. A. Rampi, *Angew. Chem. Int. Ed.* **2008**, *47*, 3407.
[14] B. Y. Choi, S. J. Kahng, S. Kim, H. Kim, H. W. Kim, Y. J. Song, J. Ihm, Y. Kuk, *Phys. Rev. Lett.* **2006**, *96*, 156106.
[15] M. Alemani, M. V. Peters, S. Hecht, K. H. Rieder, F. Moresco, L. Grill, *J. Am. Chem. Soc.* **2006**, *128*, 14446.
[16] M. Min, G. S. Bang, H. Lee, B. C. Yu, *Chem. Commun.* **2010**, *46*, 5232.
[17] W. Wang, T. Lee, M. A. Reed, *Rep. Prog. Phys.* **2005**, *68*, 544.
[18] C.-W. Chang, Y.-C. Lu, T.-T. Wang, E. W.-G. Diau, *J. Am. Chem. Soc.* **2004**, *126*, 10109.
[19] Y. Hirose, H. Yui, T. Sawada, *J. Phys. Chem. A* **2002**, *106*, 3067.
[20] C. Zhang, M. H. Du, H. P. Cheng, X. G. Zhang, A. E. Roitberg, J. L. Krause, *Phys. Rev. Lett.* **2004**, *92*, 158301.
[21] A. Noy, C. H. Sanders, D. V. Vezenov, S. S. Wong, C. M. Lieber, *Langmuir* **1998**, *14*, 1508.
[22] G. S. Bang, H. Chang, J.-R. Koo, T. Lee, R. C. Advincula, H. Lee, *Small* **2008**, *4*, 1399.
[23] R. E. Holmlin, R. Haag, M. L. Chabinyc, R. F. Ismagilov, A. E. Cohen, A. Terfort, M. A. Rampi, G. M. Whitesides, *J. Am. Chem. Soc.* **2001**, *123*, 5075.
[24] W. Wang, T. Lee, M. A. Reed, *Phys. Rev. B* **2003**, *68*, 354161.
[25] T. Li, J. R. Hauptmann, Z. Wei, S. Petersen, N. Bovet, T. Vosch, J. Nygãrd, W. Hu, Y. Liu, T. Bj rnholm, K. N rgaard, B. W. Laursen, *Adv. Mater.* **2012**, *24*, 1333.
[26] E. Bekyarova, M. E. Itkis, P. Ramesh, C. Berger, M. Sprinkle, W. A. de Heer, R. C. Haddon, *J. Am. Chem. Soc.* **2009**, *131*, 1336.
[27] H. Zhu, P. Huang, L. Jing, T. Zuo, Y. Zhao, X. Gao, *J. Mater. Chem.* **2012**, *22*, 2063.
[28] A. Salomon, D. Cahen, S. Lindsay, J. Tomfohr, V. B. Engelkes, C. D. Frisbie, *Adv. Mater.* **2003**, *15*, 1881.
[29] I. K. Moon, J. Lee, R. S. Ruoff, H. Lee, *Nat. Commun.* **2010**, *1*, 73.
[30] S. Seo, C. Jin, Y. R. Jang, J. Lee, S. K. Kim, H. Lee, *J. Mater. Chem.* **2011**, *21*, 5805.
[31] Y. Yoon, S. Seo, G. Kim, H. Lee, *Chem. Eur. J.* **2012**, *18*, 13466.